Flow Regime Based Heat Transfer Correlation for R245fa in a 3 mm Tube

Marijn Billiet[a], Bernd Ameel[a], Romain Charnay, Rémi Revellin[b], Michel De Paepe[a]

[a] *Department of Flow, Heat and Combustion Mechanics, Ghent University, Sint-Pietersnieuwstraat 41, 9000 Ghent, Belgium*
[b] *Univ Lyon, CNRS, INSA-Lyon, Université Claude Bernard Lyon 1, CETHIL UMR5008, F-69621, Villeurbanne, France*

Abstract

241 heat transfer measurements for R254fa were conducted. The heat transfer coefficient was determined for a smooth stainless steel tube with an inner tube diameter of 3 mm. The experiments were conducted for five mass fluxes (100, 300, 500, 700 and 1000 $kg/(m^2 \cdot s)$), three heat fluxes (10, 30 and 50 W/m^2) and at three saturation temperatures (40 °C, 70 °C and 125 °C). The experiments were used to determine the influence of the saturation temperature, mass flux, heat flux, vapour quality and flow regime on the heat transfer coefficient.

At a low saturation temperature, the heat transfer coefficient increases with an increasing mass flux. However, at a high saturation temperature the heat transfer coefficient decreases with an increasing mass flux. Furthermore, the heat transfer coefficient increases with increasing vapour quality at a low saturation temperature. On the contrary, the heat transfer coefficient decreases at higher saturation temperatures.

Due to the fact that most heat transfer models found in literature are developed for low saturation temperatures and one flow regime, the heat transfer coefficients predicted by the existing models do not comply very well with the experimental data. Thus, a new heat transfer correlation for R254fa was proposed. The new correlation has a Mean Absolute Error of 11.7% for the experimental data of a tube with an inner tube diameter of 3 mm. Finally, this new correlation was also verified with R245fa datasets of other authors.

Keywords: two-phase, refrigerant, heat transfer measurement

1. Introduction

The use of Organic Rankine Cycles (ORCs) can help us to reduce the global CO_2-emissions. ORCs convert low-grade heat into mechanical energy. Some typical applications of ORCs are waste heat recovery and producing electricity of geothermal energy, solar energy or biomass [1, 2]. An ORC is a Rankine cycle which uses an organic fluid instead of steam. A typical example of an organic fluid used in ORCs is R245fa [3, 4].

A Rankine cycle consists of 4 components: a pump, an evaporator, an expander and a condenser. The pump pressurises the liquid working fluid. This pressurised liquid is then evaporated at a high temperature in the evaporator. Next, the organic vapour is expanded over the expander which produces mechanical energy. Finally the vapour is condensed in the condenser. In order to size the evaporator of an ORC correctly, a good heat transfer correlation is needed. If the evaporator is not sized correctly, this will either impair the ORC's performance or increase the construction cost [5].

In literature a large variety of heat transfer correlations exist [6, 7, 8, 9]. Each correlation is based on experimental data within a certain range of working conditions. Hence, it is not certain if the correlation will work outside this range. Charnay et al. [10] compared his experimental results (R245fa) with existing heat transfer correlations. None of the tested existing heat transfer correlations could predict the heat transfer coefficient very well at the high saturation temperatures relevant for ORCs according to the authors.

The aim of this work is to present unpublished experimental heat transfer measurements of R245fa in a tube with an inner diameter of 3 mm. These measurements expand the dataset of Charnay et al. [11]. Further, the influence of the saturation temperature, mass flux, heat flux and vapour quality on the heat transfer coefficient was analysed. Finally a new heat transfer correlations was proposed.

2. Experimental setup

The experimental setup and its validation is described more detailed in [12, 11]. A short summary is given here for completeness. The experimental setup was designed to test R245fa at a saturation temperature of 40 °C to 130 °C.

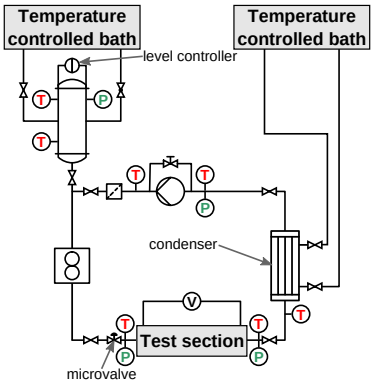

Figure 1: A schematic representation of the experimental setup. (T = temperature measurement; P = pressure measurement)

Figure 1 shows a schematic representation of the experimental setup. R245fa is pumped through a filter/dryer, a Coriolis flowmeter, a micro-valve, a test section and a condenser. The micro-valve is used to avoid oscillation when boiling

starts in the test section. Furthermore, the mass flow rate is controlled by the micro-valve together with a frequency-controlled pump and a bypass valve. The circuit also contains a temperature controlled reservoir which allows to set the saturation pressure inside the experimental setup. The whole experimental setup is controlled by a computer using Labview.

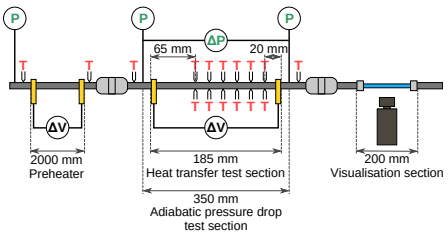

Figure 2: A detailed schematic diagram of the test section. (T = temperature measurement; P = pressure measurement; ΔV = DC power supply with voltage and current measurement)

Figure 2 shows a detail of the test section. The test section consists of a preheater, an evaporator and a visualisation section. The preheater heats up the subcooled liquid to the required vapour quality. The preheater is a 2000 mm-long spirally-shaped stainless steel tube. The actual heat transfer and adiabatic pressure drop measurements are conducted in the evaporator. The evaporator is a 185 mm-long stainless steel tube. The inner and outer diameter of both tubes are respectively 3.00 mm and 5.99 mm. Both the preheater and the evaporator are heated using the Joule effect. To electrically insulate both sections from each other and the rest of the circuit, PEEK-resin tubes are used to connect the tubes. The temperatures at the in- and outlet of the preheater are measured by two K-type thermocouples ($D_j = 0.5\,\mathrm{mm}$). The bottom- and top-wall temperatures are measured at six positions along the evaporator by K-type thermocouples ($D_j = 80\,\mu\mathrm{m}$). The same thermocouples are also used to measure the top-wall temperature at the in- and outlet of the evaporator. The differential pressure over the evaporator is measured by 3 in-range-overlapping pressure sensors.

The visualisation section at the end of the test section is used to visually determine the flow regime using a high speed camera. The images are post-processed using a Matlab algorithm. The glass tube has respectively an inner and outer diameter of 2.96 mm and 5.95 mm.

2.1. Test procedure

The experiments where conducted with R245fa for five mass fluxes (100, 300, 500, 700 and 1000 $\mathrm{kg/(m^2{\cdot}s)}$), three heat fluxes (10, 30 and 50 $\mathrm{W/m^2}$) and at three saturation temperatures (40 °C, 70 °C and 125 °C). These experiments expand the temperature range of the dataset of Charnay et al. [11] (60 °C - 120 °C).

Table 1: Overview of the experimental uncertainty of the experimental setup.

Parameter		TestRange	Uncertainty
d_i	[mm]	3	±0.03
d_o	[mm]	5.99	±0.03
L_{evap}	[mm]	185	±0.1
$\dot{q}_{ph}$	[kW/m^2]	0.5 - 20	±1.2 - 5.6 %
$\dot{q}_{evap}$	[kW/m^2]	10 - 55	±2.2 - 4.6 %
T_{sat}	[°C]	40 - 125	±0.3 - 0.8
G	[kg/(m^2·s)]	100 - 1500	±2 %
x	[-]	0 - 1	±0.001 - 0.03%
α	[kW/(K·m^2]	0.6 - 27.6	±max: 36 % avg: 17 %

The error propagation used in this work is based on the book of Taylor [13]. An overview of the experimental uncertainty of the measurements is given in table 1.

$$\bar{\alpha}_1 = \frac{\dot{q}_{evap}}{\bar{T}_{wall} - T_{sat}} \tag{1}$$

$$\bar{\alpha}_2 = \text{mean}\left(\frac{\dot{q}_{evap}}{T_{wall} - T_{sat}}\right) \tag{2}$$

In this work the average heat transfer coefficient is given by equation 1. In equation 1, $\bar{T}_{wall}$ is the average wall temperature measured around the perimeter. Some authors [14] average out the different local heat transfer coefficients determined at the perimeter (equation 2).

In most cases, both definitions give similar results considering the uncertainty. However, when the difference between the wall temperatures at different positions around the perimeter increases, the results of both definitions start to deviate significantly. Furthermore, when the temperature difference between the wall and the saturated fluid decreases, the deviation gets larger. Hence, in the case of stratified flows or partial dry-out it is important to mention which definition is used.

3. Results and discussion

3.1. Stratification at high saturation temperatures

For small tube diameters, stratification of the two phases is often suppressed [15] due to the large capillary force. The tendency of stratification is often expressed using the Eötvös number (Eo) given in equation 3. The Eötvös number expresses the ratio of the gravitational force to the surface tension force. For R245fa, the Eötvös number increases more rapidly starting from a saturation temperature of 110 °C.

$$Eo = \frac{(\rho_l - \rho_g)\, g d_i^2}{\sigma} \tag{3}$$

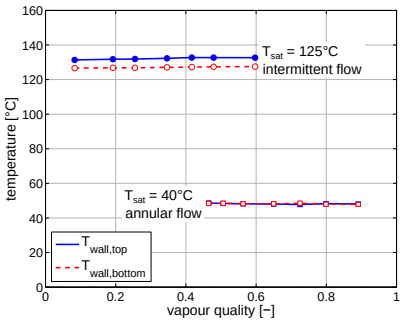

Figure 3: The wall temperature measured at the top and bottom of the tube as a function of the vapour quality for different saturation temperatures. The heat flux at the wall is 54 kW/m^2 and the mass flux is 100 kg/(m^2·s). (circle = intermittent flow; square = annular flow)

During the experiments, stratification also occurred at high saturation temperatures as seen in figure 3. Due to the stratification, there is a much thinner liquid film at the top of the tube. This thin film suppresses nucleate boiling which is a very important factor at high heat fluxes and low mass fluxes. Note that nucleate boiling occurs at the bottom part of the tube, in the liquid film which enhances the heat transfer mechanisms. Hence, the top tube wall temperature is much higher than the bottom wall temperature due to the lower local heat transfer coefficient.

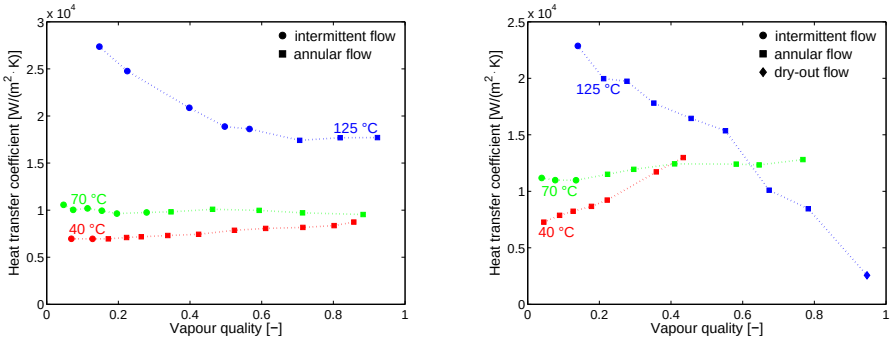

(a) G =300 kg/(m^2·s) (b) G =700 kg/(m^2·s)

Figure 4: The heat transfer coefficient as a function of the vapour quality for different saturation temperatures and a heat flux of 54 kW/m^2.

3.2. Influence of saturation temperature

In general the heat transfer coefficient increases with increasing saturation temperature as shown in Figure 4a. With increasing saturation temperature, the vapour density increases, the liquid density decreases and the surface tension

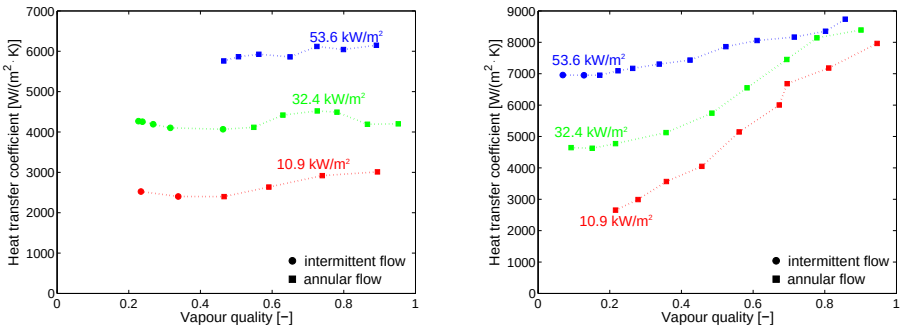

(a) G =100 kg/(m^2·s) (b) G =300 kg/(m^2·s)

Figure 5: The heat transfer coefficient as a function of the vapour quality for different heat fluxes at saturation temperature of 40 °C.

decreases for R245fa. This results in an increasing contribution of nucleate boiling to the total flow boiling heat transfer due to a decreasing bubble detachment radius and an increasing number of nucleation sites [16]. Hence, more bubbles will be formed and they will detach faster from the wall surface, enhancing the nucleate boiling heat transfer. Moreover, the decrease of vapour density with increasing saturation temperature reduces the flow velocities, reducing the convective contribution to the heat transfer. In general one can conclude that the nucleate boiling heat transfer mechanism gains in dominance with increasing saturation temperature.

However, if both the mass flux and the vapour quality are very high (see Figure 4b) previous conclusion is no longer valid. In this case, the heat transfer coefficient decreases with increasing saturation temperature. The high vapour quality thins the annular liquid film and decreases the wall superheat. This leads to a decreasing number of active nucleation sites [17] which is detrimental for the nucleate boiling heat transfer mechanism. Hence, the convective heat transfer mechanism will be the dominant one in this case. Furthermore, the increasing vapour density with increasing saturation temperature lowers the convective heat transfer. Together this explains the trend seen in Figure 4b.

3.3. Influence of heat flux

Figure 5a, 5b and 6 show that in general the heat transfer coefficient increases with increasing heat flux in the pre-dry-out region. Due to the higher heat flux, the contribution of nucleate boiling increases. During dry-out the liquid film at the wall disappears and thus also the heat transfer due to nucleate boiling. This explains also the sudden drop in Figure 6.

In general, the increase of the heat transfer coefficient with heat flux also reduces with increasing vapour quality. At higher vapour qualities, the convective heat transfer mechanism becomes more dominant and the nucleate boiling mechanism is reduced. Hence, at high vapour qualities there is a smaller effect of the heat flux on the heat transfer coefficient.

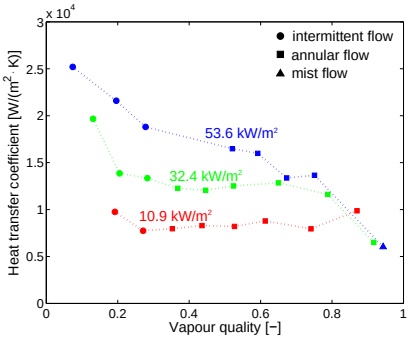

Figure 6: The heat transfer coefficient as a function of the vapour quality for different heat fluxes at saturation temperature of 125 °C and a mass flux of 500 kg/(m^2·s).

In Figure 5a (low mass flux), the nucleate boiling is the dominant heat transfer mechanism because the heat transfer coefficient does not change significantly with the vapour quality. The increasing vapour quality thins the liquid layer at the wall which reduces the number of nucleations sites due to an decrease in wall superheat. On the other hand, the contribution of the convective heat transfer mechanism increases but this increase is not large enough to compensate at higher saturation temperatures were nucleate boiling is dominant.

3.4. Influence of mass flux

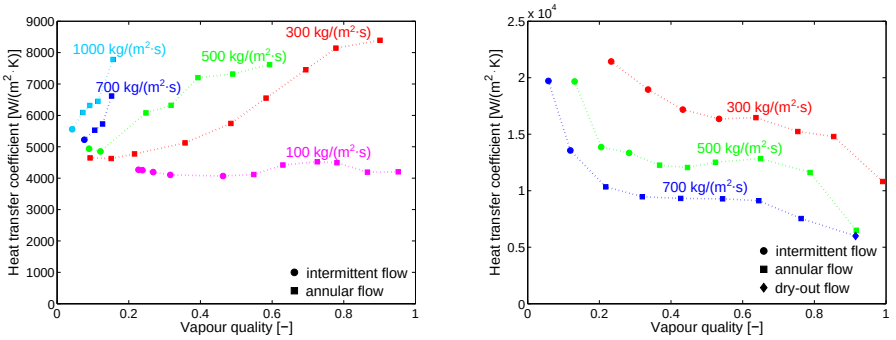

(a) T_{sat} =40 °C (b) T_{sat} =125 °C

Figure 7: The heat transfer coefficient as a function of the vapour quality for different mass fluxes and a heat flux of 32 kW/m^2.

Figure 7a and 7b show the influence of the mass flux on the heat transfer coefficient at respectively a low (40 °C) and high (125 °C) saturation temperature. At the low saturation temperature (Figure 7a), the heat transfer coefficient increases with increasing mass flux. However, the opposite is noticed at a high saturation temperature (Figure 7b). Furthermore, at a low saturation temper-

ature, the increase with increasing mass flux gets larger for increasing vapour quality.

Previous results suggest that the main heat transfer mechanism is respectively convection and nucleate boiling at a low and a high saturation temperature. The same conclusion was also found by Charnay *et al.* [11].

An increasing mass flux and vapour quality results in a increase of the flow velocity. Furthermore, the liquid film becomes thinner with increasing vapour quality. Both the increased flow velocity and the lower thermal resistance of the liquid film result in an increase of convective heat transfer. On the other hand, the thinner liquid film also lowers the superheat of the liquid film which is adversely for nucleate boiling [18, 19].

When nucleate boiling is the dominant heat transfer mechanism, the increase of the convective contribution to the heat transfer cannot compensate for the decrease of the nucleate boiling contribution.

3.5. Influence of vapour quality

At low saturation temperature (Figure 5b), an increase of the heat transfer coefficient with increasing vapour quality is noticed due to the increase of convection. However at a high saturation temperature (Figure 6), the heat transfer coefficient decreases with increasing vapour quality. The increasing vapour quality suppresses the nucleate boiling which is the dominant heat transfer mechanism at high saturation temperatures. The liquid film becomes thinner with increasing vapour quality. The thinner liquid film lowers the superheat of the liquid film which is adversely for nucleate boiling [18, 19].

At low saturation temperatures, the heat transfer coefficient increases more strongly with increasing vapour quality if the mass flux increases. However, at high saturation temperatures, the combined effect of vapour quality and mass flux is not noticeable, except in the intermittent flow regime (Figure 7b).

3.6. Heat transfer correlation

Charnay *et al.* [10] reported that none of the 29 existing heat transfer correlations they tested, worked well for predicting the results at high saturation temperatures (120 °C). The best correlation found by these authors was the correlation of Choi *et al.* [20]. This correlation is based on the correlation of Chen *et al.* [21]. In this work, the dataset of Charnay *et al.* [10] is expanded with new measurements using the same experimental setup. The measurements with an uncertainty larger than 20% are discarded from the combined dataset and only the measurements at the end of the test section are kept (i.e. the measurements from the last set of thermocouples in the test section).

The combined dataset is compared with the correlation of Choi *et al.* [20] in Figure 8. Typically the goodness of fit is expressed as a mean absolute error (MAE) or mean relative error (MRE).

$$\mathrm{MRE} = \frac{1}{n}\sum_{i=1}^{n}\left(\frac{\alpha_{pred,i} - \alpha_{exp,i}}{\alpha_{exp,i}}\right) \tag{4}$$

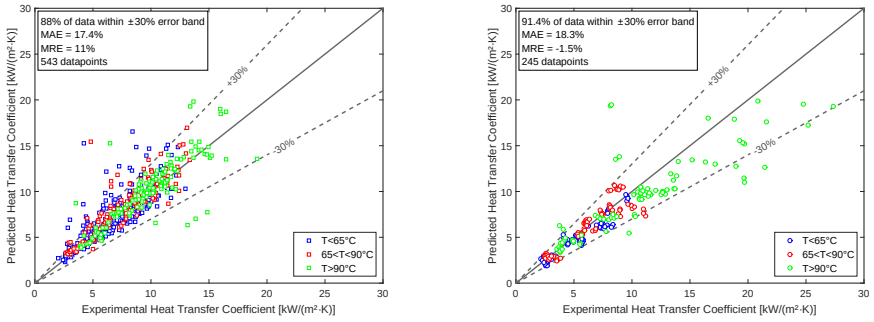

(a) Annular (b) Intermittent

Figure 8: Performance of the correlation of Choi *et al.* [20] for the combined dataset (dataset of Charnay *et al.* [11] and new experiments) for Annular and Intermittent flow

$$\mathrm{MAE} = \frac{1}{n}\sum_{i=1}^{n}\left|\frac{\alpha_{pred,i} - \alpha_{exp,i}}{\alpha_{exp,i}}\right| \tag{5}$$

In Figure 8 no distinctive difference in fitting quality between different saturation temperatures can be seen as stated by Charnay *et al.* [11]. However, there is a difference between the annular and the intermittent flow. The correlation of Choi *et al.* [20] overpredicts the annular flow experiments on average by 11% and underpredicts the intermittent flow experiments on average by 1.5%. To correct this, a new correlation is proposed. A flow regime dependency will be added to the correlation of Choi *et al.* [20].

The new correlation (equation 6) is a weighted average of the heat transfer coefficient of an annular flow and the one of an intermittent flow. This weighted average keeps the correlation smooth across the flow regime boundaries.

$$\begin{aligned}\alpha = {} & (\mathrm{P\,[A]})\ (S_A\,\alpha_{nb} + F_A\,\alpha_{cb}) \\ & + (1 - \mathrm{P\,[A]})\ (S_I\,\alpha_{nb} + F_I\,\alpha_{cb})\end{aligned} \tag{6}$$

The weighing is accomplished using the probability of the flow being annular (P [A]). This probability is calculated using the probabilistic flow pattern maps of Canière et al. [22] (equations 7 to 8).

$$Fr_l = \frac{G^2}{\rho_l^2 \cdot g \cdot d} = C\ (X_{tt})^n \tag{7}$$

$$n = -0.618\ (\mathrm{P\,[A]})^2 + 0.6975\,\mathrm{P\,[A]} + 2.504 \tag{8}$$

$$X_{tt} = \left(\frac{1-x}{x}\right)^{0.9}\sqrt{\frac{\rho_g}{\rho_l}}\left(\frac{\mu_l}{\mu_g}\right)^{0.1} \tag{9}$$

$$C = 14.27\,\mathrm{P\,[A]} + 2.315 \tag{10}$$

For both the annular and intermittent flow, the heat transfer coefficient for nucleate boiling (α_{nb}) is calculated using the correlation of Cooper [23].

$$\alpha_{nb} = 55\, \dot{q}^{0.67}\, p_r^{0.12}\, M^{-0.5}\, \left(-\log\left(p_r\right)\right)^{-0.55} \tag{11}$$

Further, the heat transfer coefficient for convective boiling (α_{cb}) is calculated using the correlation of Dittus and Boelter [24] for both flow regimes.

$$\alpha_{cb} = 0.023\, \frac{k_l}{d_i} \left(\frac{G\,(1-x)\,d_i}{\mu_l}\right)^{0.8} \left(\frac{C_{p,l}\,\mu_l}{k_l}\right)^{0.4} \tag{12}$$

Table 2: The coefficients of the flow enhancing and boiling suppression factor for an annular and intermittent flow.

	a_1	a_2	a_3	a_4	a_5	a_6
I	0.95	0.05	1	7.2694	0.0094	0.2814
A	0	0.33	0.654	9.48	−0.072	0.3003

For both the annular flow and intermittent flow, the flow enhancing factor F and the nucleate boiling suppression factor S are calculated using equations 13 and 14, respectively. The parameters a_i are found in table 2 for both the intermittent flow and the annular flow. The parameters a_i for the intermittent flow are the same as the original version of Choi *et al.* [20]. The ones for the annular flow are found by fitting the combined dataset.

$$F = a_1 + a_2\, \left(\phi^2\right)^{a_3} \tag{13}$$

$$S = a_4\, \left(\phi^2\right)^{a_5}\, Bo^{a_6} \tag{14}$$

$$Bo = \frac{\dot{q}}{G\, h_{lg}} \tag{15}$$

$$\phi^2 = 1 + \frac{C'}{X} + \frac{1}{X^2} \tag{16}$$

$$C' = \begin{cases} 5 & Re_l \leq 1000 \text{ and } Re_g \leq 1000 \\ 10 & Re_l \geq 2000 \text{ and } Re_g \leq 1000 \\ 12 & Re_l \leq 1000 \text{ and } Re_g \geq 2000 \\ 20 & Re_l \geq 2000 \text{ and } Re_g \geq 2000 \\ \text{interpolation} & \text{other} \end{cases} \tag{17}$$

$$X = \left(\frac{\mu_l}{\mu_g}\right)^{1/8} \left(\frac{1-x}{x}\right)^{7/8} \sqrt{\frac{\rho_g}{\rho_l}} \tag{18}$$

Before the parameters a_i are determined by fitting the combined dataset, there is checked for both flow regimes if all coefficients are significant. The combined dataset is split up according to the flow regime determined using the high speed footage. For both flow regimes the parameters a_i of the original

correlation of Choi *et al.* [20] are refitted. Then one parameter at a time was varied and kept constant while the other parameters were refitted. The result is is shown in Figure 9. The figure gives one minus the Coefficient of determination (r squared value) as a function of the parameter which was kept constant.

In case of the annular flow all coefficients are important because the best fit cannot be reached with a random value for one of the parameters. For the intermittent flow, parameter a_3 is not significant because the goodness of fit does not change with the change of parameter a_3. Due to the weighted average used in the final correlation, there was chosen to keep parameter a_3 in the intermittent part of the new correlation. The intermittent part of the new correlation will still have a large influence if the flow is for example 60% annular according to the probabilistic flow pattern maps of Canière et al. [22].

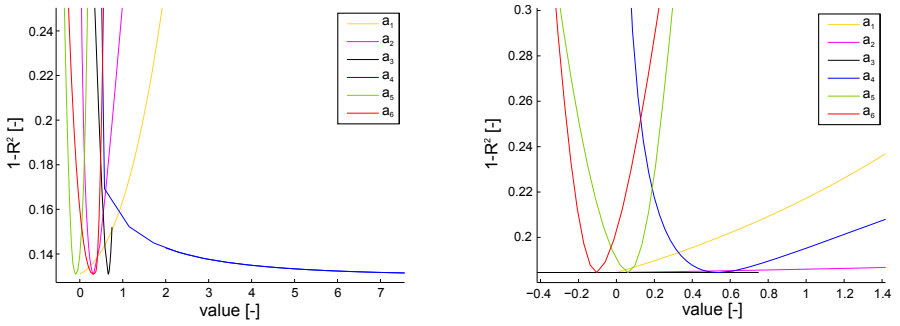

(a) Annular (b) Intermittent

Figure 9: One minus the Coefficient of determination of the original correlation of Choi *et al.* [20] as a function of the value of the parameter which is kept constant while the other parameters are refitted to the dataset.

The new correlation is compared with the original correlation of Choi *et al.* [20] in Figure 10. The MAE and MRE is reduced to 11.7% and 0.292% respectively. The MRE is almost zero which means that there is on average no under- or overprediction.

Table 3: The performance of the new correlation for other R245fa datasets in literature. (o = original correlation of Choi *et al.* [20]; n = new correlation; $EB_{20\%}$ = number of measurements within the 20% error band)

	d_i [mm]	MAE_o [-]	MAE_n [-]	MRE_o [-]	MRE_n [-]	$EB_{20\%,o}$	$EB_{20\%,n}$
Bortolin *et al.* [25]	0.96	0.301	0.181	0.148	0.0165	10 of 18	13 of 18
Pike-Wilson *et al.* [26]	1.1	0.668	0.629	0.171	0.125	87 of 346	93 of 346
Consolini *et al.* [27]	0.5-0.8	0.264	0.234	0.257	0.226	33 of 72	33 of 72
Ong *et al.* [28]	1	0.272	0.236	0.227	0.189	36 of 98	46 of 98
Tibirica *et al.* [14]	2.3	0.711	0.200	0.549	0.0644	59 of 90	72 of 90

Finally, this new correlation was also verified with R245fa datasets of other

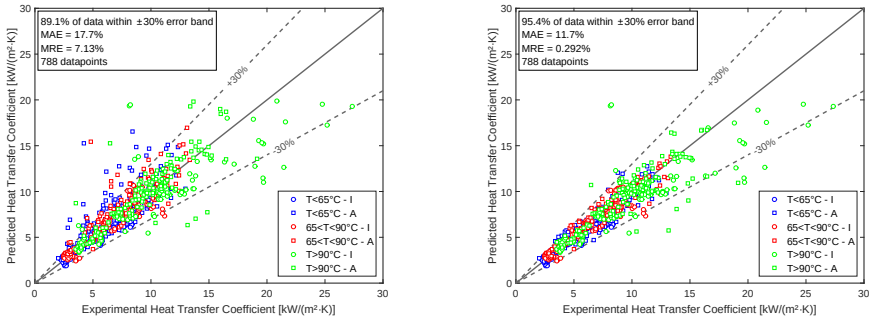

(a) Original [20] (b) adapted correlation

Figure 10: Performance of the original and adapted version of the correlation of Choi *et al.* [20] for the combined dataset. (I = Intermittent flow; A = Annular flow)

authors. The improvement of the MRE and MAE can be found in table 3. In general, the fit of all datasets improves. However, only the set of Tibirica et al. [14] improves significantly. This is also the only dataset with a similar tube diameter. Furthermore, 71% of the data points are annular flow when the flow pattern map of Kattan *et al.* [29] is used. The other sets have much smaller tube diameters and are actually micro-tubes where the effect of surface tension gains importance.

4. Conclusions

This work presented 241 unpublished experimental heat transfer measurements of R245fa in a tube with an inner diameter of 3 mm and discussed the influence of the saturation temperature, mass flux, heat flux and vapour quality on the heat transfer coefficient.

The heat transfer coefficient respectively increased and decreased with an increasing mass flux at a low and high saturation temperature. Furthermore, the heat transfer coefficient increased with increasing vapour quality at a low saturation temperature. On the contrary, the heat transfer coefficient decreased at higher saturation temperatures. Hence, the influence of vapour quality and mass flux on the heat transfer coefficient is dependent of the saturation temperature.

The combined dataset of this work (241 data points) and Charnay et al. [10] (973 data points) is best predicted by the correlation of Choi *et al.* [20]. However, the experimental data of the annular flow is overpredicted. A new flow regime dependant correlation for R245fa was proposed. The new correlation is experimentally validated for tubes with an inner diameter of 3 mm, a temperature range of 40 °C to 125 °C, a mass flux between 100 $\mathrm{kg/(m^2{\cdot}s)}$ and 1000 $\mathrm{kg/(m^2{\cdot}s)}$ and a heat flux between 10 $\mathrm{W/m^2}$ and 50 $\mathrm{W/m^2}$. Finally, this new correlation was also verified with R245fa datasets of other authors.

Nomenclature

avg	average	Bo	Boiling number
C_p	specific heat capacity	d	diameter
Eo	Eötvös number	F	flow enhancement factor
Fr	Froude number	G	mass flux
g	standard gravity	h_{lg}	latent heat
k	thermal conductivity	L	length
M	molar mass	MAE	mean absolute error
max	maximum	MRE	mean relative error
P	pressure	P [A]	probability of an annular flow
p_r	relative pressure ($= \frac{P_{sat}}{P_{crit}}$)	$\dot{q}$	heat flux
R^2	coefficient of determination	S	boiling suppression factor
T	temperature	x	vapour quality
X	Lockhart-Martinelli parameter	X_{tt}	turbulent Lockhart-Martinelli parameter

Greek symbols

α	heat transfer coefficient	ρ	density
ϕ^2	two-phase frictional multiplier	μ	dynamic viscosity

Subscripts

A	annular	I	intermittent
cb	convective boiling	l	liquid
$crit$	critical	nb	nucleate boiling
$evap$	evaporator	o	outer
exp	experimental	ph	preheater
g	gas	$pred$	predicted
i	inner	sat	saturation

Acknowledgement

Research funded by a Ph.D. grant (nr. 141733) of the Agency for Innovation by Science and Technology (IWT) and a CWO travel grant of Ghent University.

References

[1] B. F. Tchanche, G. Lambrinos, A. Frangoudakis, G. Papadakis, Low-grade heat conversion into power using organic rankine cycles – a review of various applications, Renewable and Sustainable Energy Reviews 15 (8) (2011) 3963–3979. doi:10.1016/j.rser.2011.07.024.

[2] E. H. Wang, H. G. Zhang, B. Y. Fan, M. G. Ouyang, Y. Zhao, Q. H. Mu, Study of working fluid selection of organic rankine cycle (orc) for engine waste heat recovery, Energy 36 (6) (2011) 3406–3418. doi:10.1016/j.energy.2011.03.041.

[3] S. Lecompte, H. Huisseune, M. van den Broek, M. De Paepe, Methodical thermodynamic analysis and regression models of organic rankine cycle architectures for waste heat recovery, Energy 87 (2015) 60–76. doi:10.1016/j.energy.2015.04.094.

[4] B. Saleh, G. Koglbauer, M. Wendland, J. Fischer, Working fluids for low-temperature organic rankine cycles, Energy 32 (2007) 1210–1221. doi:10.1016/j.energy.2006.07.001.

[5] A. Kaya, M. Lazova, S. Lecompte, M. De Paepe, Design sensitivity analysis of a direct evaporator for low-temperature waste heat recovery orcs using various flow boiling heat transfer correlations, in: ICR2015, Proceedings, 2015.

[6] A. Kaya, M. Lazova, Ö. Bağci, S. Lecompte, B. Ameel, M. De Paepe, Design sensitivity analysis of a plate-finned air-cooled condenser for low-temperature organic rankine cycles, HEAT TRANSFER ENGINEERING 37. doi:10.1080/01457632.2016.1216966.

[7] N. Kattan, J. R. Thome, D. Favrat, Flow boiling in horizontal tubes: Part 3 – development of a new heat transfer model based on flow pattern, Journal of Heat Transfer 120 (1) (1998) 156–165. doi:10.1115/1.2830039.

[8] W. Li, Z. Wu, A general correlation for evaporative heat transfer in micro/mini-channels, International Journal of Heat and Mass Transfer 53 (9-10) (2010) 1778–1787. doi:10.1016/j.ijheatmasstransfer.2010.01.012.

[9] F. T. Kanizawa, C. B. Tibiri, G. Ribatski, Heat transfer during convective boiling inside microchannels, International Journal of Heat and Mass Transfer 93 (2016) 566–583. doi:10.1016/j.ijheatmasstransfer.2015.09.083.

[10] R. Charnay, R. Revellin, J. Bonjour, Flow boiling heat transfer in minichannels at high saturation temperatures: Part II – assessment of predictive methods and impact of flow regimes, International Journal of Heat and Mass Transfer 87 (2015) 653–672. doi:10.1016/j.ijheatmasstransfer.2015.03.080.

[11] R. Charnay, R. Revellin, J. Bonjour, Flow boiling heat transfer in minichannels at high saturation temperatures: Part I – experimental investigation and analysis of the heat transfer mechanisms, International Journal of Heat and Mass Transfer 87 (2015) 636–652. doi:10.1016/j.ijheatmasstransfer.2015.03.081.

[12] R. Charnay, Experimental study of flow boiling in horizontal minichannels at high saturation temperature, PhD dissertation, Institut National des Sciences Appliquées de Lyon (February 2014).
URL `http://theses.insa-lyon.fr/publication/2014ISAL0047/these.pdf`

[13] J. R. Taylor, An Introduction to Error Analysis: The Study of Uncertainties in Physical Measurements, 2nd Edition, University Science Books, 1997.

[14] C. B. Tibiriçá, G. Ribatski, Flow boiling heat transfer of R134a and R245fa in a 2.3mm tube, International Journal of Heat and Mass Transfer 53 (11-12) (2010) 2459–2468. doi:10.1016/j.ijheatmasstransfer.2010.01.038.

[15] J. W. Coleman, S. Garimella, Characterization of two-phase flow patterns in small diameter round and rectangular tubes, International Journal of Heat and Mass Transfer 42 (15) (1999) 2869–2881. doi:10.1016/S0017-9310(98)00362-7.

[16] D. Gorenflo, U. Chandra, S. Kotthoff, A. Luke, Influence of thermophysical properties on pool boiling heat transfer of refrigerants, International Journal of Refrigeration 27 (5) (2004) 492–502. doi:10.1016/j.ijrefrig.2004.03.004.

[17] C. Dang, N. Haraguchi, E. Hibara, Flow boiling heat transfer of carbon dioxide inside a small-sized microfin tube, International Journal of Refrigeration 33 (4) (2010) 655–663. doi:10.1016/j.ijrefrig.2010.01.003.

[18] A. Cioncolini, J. R. Thome, Prediction of the entrained liquid fraction in vertical annular gas-liquid two-phase flow, International Journal of Multiphase Flow 36 (4) (2010) 293–302.

[19] M. Ducoulombier, S. Colasson, J. Bonjour, P. Haberschill, Carbon dioxide flow boiling in a single microchannel – part II: Heat transfer, Experimental Thermal and Fluid Science 35 (2011) 597–611. doi:10.1016/j.expthermflusci.2010.11.014.

[20] K. Choi, A. Pamitran, J.-T. Oh, Two-phase flow heat transfer of CO2 vaporization in smooth horizontal minichannels, International Journal of Refrigeration 30 (2007) 767–777. doi:10.1016/j.ijrefrig.2006.12.006.

[21] J. C. Chen, Correlation for boiling heat transfer to saturated fluids in convective flow, Industrial & Engineering Chemistry Process Design and Development 5 (3) (1966) 322–329. doi:10.1021/i260019a023.

[22] H. Canière, B. Bauwens, C. T'Joen, M. De Paepe, Mapping of horizontal refrigerant two-phase flow patterns based on clustering of capacitive sensor signals, International Journal of Heat and Mass Transfer 53 (2010) 5298–5307. doi:10.1016/j.ijheatmasstransfer.2010.07.027.

[23] M. G. Cooper, Heat flow rates in saturated nucleate pool boiling – a wide-ranging examination using reduced properties, Advances in Heat Transfer 16 (1984) 157–239.

[24] F. Dittus, L. Boelter, Heat transfer in automobile radiators of the tubular type, International Communications in Heat and Mass Transfer 12 (1) (1985) 3–22. doi:http://dx.doi.org/10.1016/0735-1933(85)90003-X.

[25] S. Bortolin, D. Del Col, L. Rossetto, Flow boiling of R245fa in a single circular microchannel, in: Second Micro and Nano Flows Conference, 2009.

[26] E. A. Pike-Wilson, T. G. Karayiannis, Flow boiling of R245fa in 1.1mm diameter stainless steel, brass and copper tubes, Experimental Thermal and Fluid Science 59 (2014) 166–183. doi:10.1016/j.expthermflusci.2014.02.024.

[27] L. Consolini, J. R. Thome, Micro-channel flow boiling heat transfer of R-134a, R-236fa, and R-245fa, Microfluidics and Nanofluidics 6 (6) (2009) 731–746. doi:10.1007/s10404-008-0348-7.

[28] C. L. Ong, J. R. Thome, Flow boiling heat transfer of R134a, R236fa and R245fa in a horizontal 1.030mm circular channel, Experimental Thermal and Fluid Science 33 (4) (2009) 651–663. doi:10.1016/j.expthermflusci.2009.01.002.

[29] N. Kattan, J. Thome, D. Favrat, Flow boiling in horizontal tubes: Part 1 – development of a diabatic two-phase flow pattern map, Journal of Heat Transfer 120 (1) (1998) 140–147.